

## Modeling mechanophore activation within a crosslinked glassy matrix

Meredith N. Silberstein, Kyoungmin Min, Lee D. Cremar, Cassandra M. Degen, Todd J. Martinez et al.

Citation: *J. Appl. Phys.* **114**, 023504 (2013); doi: 10.1063/1.4812581

View online: <http://dx.doi.org/10.1063/1.4812581>

View Table of Contents: <http://jap.aip.org/resource/1/JAPIAU/v114/i2>

Published by the [AIP Publishing LLC](#).

---

### Additional information on *J. Appl. Phys.*

Journal Homepage: <http://jap.aip.org/>

Journal Information: [http://jap.aip.org/about/about\\_the\\_journal](http://jap.aip.org/about/about_the_journal)

Top downloads: [http://jap.aip.org/features/most\\_downloaded](http://jap.aip.org/features/most_downloaded)

Information for Authors: <http://jap.aip.org/authors>

## ADVERTISEMENT



**AIPAdvances**

Now Indexed in  
Thomson Reuters  
Databases

Explore AIP's open access journal:

- Rapid publication
- Article-level metrics
- Post-publication rating and commenting

## Modeling mechanophore activation within a crosslinked glassy matrix

Meredith N. Silberstein,<sup>1,a)</sup> Kyoungmin Min,<sup>1,2</sup> Lee D. Cremar,<sup>3</sup> Cassandra M. Degen,<sup>4</sup> Todd J. Martinez,<sup>3</sup> Narayana R. Aluru,<sup>1,2</sup> Scott R. White,<sup>1,5</sup> and Nancy R. Sottos<sup>1,4</sup>

<sup>1</sup>Beckman Institute for Advanced Science and Technology, University of Illinois at Urbana-Champaign, Urbana, Illinois 61801, USA

<sup>2</sup>Department of Mechanical Science and Engineering, University of Illinois at Urbana-Champaign, Urbana, Illinois 61801, USA

<sup>3</sup>Department of Chemistry, Stanford University, Stanford, California 94305, USA

<sup>4</sup>Department of Materials Science and Engineering, University of Illinois at Urbana-Champaign, Urbana, Illinois 61801, USA

<sup>5</sup>Department of Aerospace Engineering, University of Illinois at Urbana-Champaign, Urbana, Illinois 61801, USA

(Received 16 April 2013; accepted 14 June 2013; published online 8 July 2013)

Mechanically induced reactivity is a promising means for designing self-reporting materials. Mechanically sensitive chemical groups called mechanophores are covalently linked into polymers in order to trigger specific chemical reactions upon mechanical loading. These mechanophores can be linked either within the backbone or as crosslinks between backbone segments. Mechanophore response is sensitive to both the matrix properties and placement within the matrix, providing two avenues for material design. A model framework is developed to describe reactivity of mechanophores located as crosslinks in a glassy polymer matrix. Simulations are conducted at the molecular and macromolecular scales in order to develop macroscale constitutive relations. The model is developed specifically for the case of spiropyran (SP) in lightly crosslinked polymethylmethacrylate (PMMA). This optically trackable mechanophore (fluorescent when activated) allows the model to be assessed in terms of observed experimental behavior. The force modified potential energy surface (FMPEs) framework is used in conjunction with *ab initio* steered molecular dynamics (MD) simulations of SP to determine the mechanophore kinetics. MD simulations of the crosslinked PMMA structure under shear deformation are used to determine the relationship between macroscale stress and local force on the crosslinks. A continuum model implemented in a finite element framework synthesizes these mechanochemical relations with the mechanical behavior. The continuum model with parameters taken directly from the FMPEs and MD analyses under predicts stress-driven activation relative to experimental data. The continuum model, with the physically motivated modification of force fluctuations, provides an accurate prediction for monotonic loading across three decades of strain rate and creep loading, suggesting that the fundamental physics are captured. © 2013 AIP Publishing LLC.

[<http://dx.doi.org/10.1063/1.4812581>]

### I. BACKGROUND

Mechanically sensitive chemical groups termed mechanophores are covalently linked into polymers in order to trigger specific chemical reactions upon mechanical loading. Mechanophores present a novel means for designing multifunctional and smart materials. The mechanophore reactions take place as a result of the transmission of stress on the macroscale to force on the molecular scale. Mechanophores are responsive in a range of polymer matrices and modes of macroscopic deformation (Hickenboth *et al.*, 2007; Caruso *et al.*, 2009; Davis *et al.*, 2009; Lee *et al.*, 2010; Black *et al.*, 2011; Beiermann *et al.*, 2011; Kingsbury *et al.*, 2011). The strain and corresponding stress at which mechanophores activate, as well as the subsequent evolution in activation, depend heavily on the polymer matrix and linking architecture. In glassy polymers, molecular mobility is a major

restriction on activation, with mechanophores only responding during plastic deformation.

Here, a microstructurally based model is developed to describe the response of mechanophores within glassy polymers. This model is conceptually similar to one developed by the authors for mechanophore activation in elastomers (Silberstein *et al.*, personal communication). However, the transmission of stress at the macro scale down to force at the mechanophore is significantly different for glassy polymers than for elastomers. Molecular dynamics (MD) simulations are used here to make the connection from macroscopic stress to local force. The mechanochemically coupled continuum model synthesizes information about the macro scale mechanical response, the transmission of stress to local force, and force dependent mechanophore kinetics.

### II. METHODS

The continuum activation model developed herein relies on two smaller scale simulation methods (molecular

<sup>a)</sup>Author to whom correspondence should be addressed. Electronic mail: ms2682@cornell.edu

dynamics for local force and *ab initio* calculations for mechanophore kinetics) and a continuum mechanical model. The methods for each of these simulations are presented below along with the specific material and experiments for which these simulations are tailored.

### A. Materials

The material investigated is a crosslinked poly(methyl methacrylate) (PMMA) with a total crosslink density of 1 mol. %. PMMA samples are crosslinked with a primary crosslinker of ethylene glycol dimethacrylate (EGDMA) (0.982 mol. %) and a secondary crosslinker of spiropyran (SP) (0.018 mol. %) (Kingsbury *et al.*, 2011). The mechanophore SP undergoes a ring opening reaction to the merocyanine (MC) form through application of force or UV light and can be reversed by visible light. The theoretical characteristic length of EGDMA is 0.8 nm, whereas SP is 0.7 nm and MC is 1.3 nm (Davis *et al.*, 2009).

### B. Experimental characterization

Measurements for torque, rotation, and fluorescence intensity are captured simultaneously during torsional testing (Kingsbury *et al.*, 2011; Kingsbury *et al.*, 2012). The solid torsion sample has a gauge section 2 mm in diameter and 10 mm long. Monotonic torsion tests are conducted at constant rotational rates of  $10^{-3}$ ,  $10^{-2}$ , and  $10^{-1}$  rad s $^{-1}$ . Creep torsional tests are loaded at a constant rotational rate of  $10^{-2}$  rad s $^{-1}$  until a target torque is reached at which point the torque is held constant until specimen fracture.

The raw rotation and torque data are converted into shear strain and an estimated shear stress at the outer surface of the specimen using an adaptation of Nadai's solution (Nadai, 1950) derived by Wu *et al.* (1992) to account for axial deformation

$$\gamma = r \left( 1 - \frac{1}{2} A \right) \phi, \quad (1)$$

$$\tau_o = \frac{1}{2\pi r^3} \left( 3M + \phi \frac{\partial M}{\partial \phi} \right) \left[ \frac{1}{1 - \frac{1}{2} \left( 3A + \phi \frac{\partial A}{\partial \phi} \right)} \right], \quad (2)$$

where  $\gamma$  is the shear strain,  $\tau_o$  is the shear stress at the outer surface of the sample,  $r$  is the sample radius,  $A$  is the axial strain,  $\phi$  is the angle of rotation of the specimen, and  $M$  is the applied torque.

Fluorescence is quantified via full field fluorescence imaging synchronized with the mechanical data collection (Kingsbury *et al.*, 2011). Samples are exposed to white light before testing to drive the mechanophores into the SP form. Fluorescence is excited with a white pipe light filtered to allow only 400 nm–550 nm light to pass. The output fluorescence signal is passed through a filter allowing wavelengths 600 nm–1200 nm and collected with a color camera (Basler CCD). For creep testing, the input laser light is shuttered to minimize light induced mechanophore closing. The activation (relative amount of mechanophores in the MC form as measured optically) value at any point in time/load history is determined

by comparing the full field fluorescence averaged intensity with the corresponding measurement on specimens synthesized under UV light. This normalization assumes that synthesis under UV light drives the forward reaction of SP to MC to completion.

### C. *Ab-initio* molecular dynamics (FMPES-MEP)

Mechanophore level kinetics are determined using first principles methods that incorporate external force pulling schemes. *Ab initio* steered molecular dynamics (AISMD) predicts mechanophore reactivity in response to applied forces (Ong *et al.*, 2009). This method employs a constant force scheme whereby force is applied to select atomic sites on the mechanophore, consistent with the polymer chain connection points. The AISMD simulations dynamically solve the electronic Schrödinger equation allowing arbitrary bond rearrangement. The method has the important attribute of requiring no fitting parameters, but is computationally expensive. AISMD provides information on the reaction mechanism at large forces where the simulations may span picosecond time scales. To circumvent the cost of running AISMD simulations at lower forces and longer timescales, a force modified potential energy surface (FMPES) framework is adopted. The FMPES framework consists of knowledge of the minimal energy pathway (MEP) on the potential energy surface, which contains structural information regarding the reactants, transition states, and products. The MEP which connects the minima to a transition state, is optimized at a specified force value providing information on the force perturbed geometry conformations. Additionally, knowledge of the activation barriers as a function of force is obtained along the reaction pathway. Since the MEP along the FMPES provides geometrical information (reactants, transition state), any single bond distance or angle can be monitored along the reaction coordinate. The attempt frequencies for the forward (activation) and reverse (deactivation) reaction are also determined using the FMPES framework.

Transition state theory is used to calculate reaction rates that are relevant to laboratory timescales from known force dependent activation barriers and attempt frequencies. A single reactant to single product mechanophore transformation is described by

$$\dot{\alpha} = k_f(1 - \alpha) - k_r\alpha, \quad (3)$$

where  $\alpha$  is the concentration of mechanophores in the activated (triggered) state,  $\dot{x}$  indicates a time rate of change for any variable  $x$ ,  $k_f$  is the forward reaction rate, and  $k_r$  is the reverse reaction rate. In the case of the mechanophore used here, there will be two different conformations of the final product. The pathway to each product conformation has its own rate constant

$$\dot{\alpha}_d = k_{d,f}(1 - \alpha) - k_{d,r}\alpha_d, \quad (4)$$

where the subscript  $d$  stands for either pathway 1 or pathway 2. The total activated population is the sum of the two conformations

$$\alpha = \alpha_1 + \alpha_2. \quad (5)$$

Each rate constant is expressed as follows:

$$k_{d,a} = \frac{k_b \theta Q_{d,a}^\ddagger}{h Q_{d,a}} \exp \left[ \frac{-\Delta G_{d,a}}{R\theta} \right], \quad (6)$$

where the subscript  $a$  stands for either the forward ( $f$ ) or reverse ( $r$ ) reaction,  $k_b$  is Boltzmann's constant,  $\theta$  is the absolute temperature,  $h$  is Planck's constant,  $\frac{Q_{d,a}^\ddagger}{Q_{d,a}}$  is the attempt frequency,  $\Delta G_{d,a}$  is the transformation energy barrier, and  $R$  is the universal gas constant.

When the external force is sufficiently small, the activation energy depends linearly on the external force (Kauzmann and Eyring, 1940; Bell, 1978), i.e.,

$$\Delta G_{d,a} = \Delta G_{d,a}^o + f \Delta x_{d,a}, \quad (7)$$

where  $f$  is the applied force and  $\Delta x_{d,a}$  is an effective distance between the reactant minimum and transition state geometries. We determine  $\Delta x_{d,a}$  from FMPES MEP calculations with applied force of 0 nN and 0.5 nN and use Eq. (7) to predict activation energies at all forces needed in the mesoscopic simulations. The prefactor  $\frac{Q_{d,a}^\ddagger}{Q_{d,a}}$  has a secondary influence on reaction kinetics and is also linearly interpolated based on FMPES calculations at 0 nN and 0.5 nN of applied force.

#### D. Classical MD

Molecular dynamics simulations are used to quantify the relationship between macroscopic stress and local force on the mechanophore. To that end, an EGDMA crosslinked PMMA structure, analogous to the experimentally investigated material, is subjected to shear deformation. The lightly crosslinked PMMA structure is constructed from 12 chains of linear PMMA each 252 monomer units long. This chain length (25.2 kg/mol) sufficiently exceeds the entanglement molecular weight of PMMA, around 10 kg/mol (Mark, 1996), resulting in the desired bulk entangled behavior. 1.15 mol. % EGDMA is attached to arbitrarily selected carbon backbones on the linear PMMA chains. Three dimensional periodic boundary conditions are enforced. The number of chains is selected to avoid the size dependency of the periodic box as indicated by convergence of the shear stress-strain curve.

The simulation procedure consists of first relaxing the crosslinked PMMA structure and then applying shear deformation. The structure is relaxed to a quasi-equilibrium state by annealing at high pressure (10 atm) and temperature (600 K), cooling to 300 K, and then holding at 1 atm and 300 K until a stable thermodynamic state is reached. Each set of data presented is the average result from ten different initial configurations generated by varying the relaxation time at 1 atm and 300 K. The simulations are conducted within the large-scale atomic/molecular massively parallel simulator (LAMMPS) (Plimpton, 1995). An explicit atom representation is used with atomic interactions captured by a Dreiding interatomic forcefield (Mayo, 1990). The Dreiding potential is chosen because it has been shown to accurately

capture the bulk density and glass transition temperature of amorphous linear PMMA (Sane *et al.*, 2001) and the mechanical deformation behavior of glassy polymers (Fan *et al.*, 1994; Jaramillo *et al.*, 2012). The velocity-Verlet time stepping scheme is used with a time step of 1 fs. A Nosé-Hoover thermostat is applied for temperature control. Shear deformation is applied by a constant relative displacement rate of two parallel faces of the periodic box, while maintaining pressure at 1 atm on the free faces using NPT (number of atoms, pressure, and temperature held constant) dynamics. Shear strain is calculated as  $\gamma = \Delta x/y_o$ , where  $\Delta x$  is displacement in the shear direction and  $y_o$  is the initial offset between the displacing faces. Shear stress is taken directly from the LAMMPS virial stress output for all the atoms in the structure. Average shear force across particular atoms is reduced from the LAMMPS atomic virial stress output using an estimated atomic radius of 0.1 nm.

#### E. Continuum implementation

The continuum simulations are implemented within a finite element framework using the commercial software ABAQUS. The material behavior is mathematically described within an explicit user material subroutine (vumat). Rotation is applied to a solid cylindrical specimen in order to closely match the experimentally applied conditions and response. The material definition is local with the stress in each element driving activation in that element as described in detail in Sec. III B. It is assumed that there is no feedback from the activation back to the mechanical response. An implicit Euler scheme is used to solve for the activation value within each element at each time step. Strain and stress are taken at the outer surface of the cylinder according to Eqs. (1) and (2), respectively. This output is verified with comparison to the direct finite element output at the outer surface showing only small differences. In order to best mimic the experimental setup, activation is the mean of the upper and lower bounds for activation where the upper bound is the outer surface and the lower bound is the volumetric average through the gauge section.

### III. CONTINUUM THEORY

#### A. Mechanical model

An elastic-viscoplastic model is used to capture the rate dependent mechanical behavior of crosslinked PMMA. This model draws its main concepts from the prior PMMA models of Srivistava *et al.* (2010) and Mulliken and Boyce (2006). These models are chosen for their accurate description of rate dependent yield peak, an essential feature for the subsequent activation model. Network contributions to the stress are incorporated into the elastic-viscoplastic model as isotropic hardening in order to simplify the mechanical model formulation.

##### 1. Kinematics

The total deformation gradient is multiplicatively decomposed into elastic ( $\mathbf{F}^e$ ) and plastic ( $\mathbf{F}^p$ ) components

$$\mathbf{F} = \mathbf{F}^e \mathbf{F}^p. \quad (8)$$

Plastic deformation is assumed to be incompressible such that  $J^p = \det \mathbf{F}^p = 1$ .

For later use, the elastic deformation gradient is decomposed into stretch ( $\mathbf{V}^e$ ) and rotation ( $\mathbf{R}^e$ ) components

$$\mathbf{F}^e = \mathbf{V}^e \mathbf{R}^e. \quad (9)$$

The rate kinematics are described by the velocity gradient  $\mathbf{L} \equiv \dot{\mathbf{F}}\mathbf{F}^{-1}$ , which can be decomposed into its elastic ( $\mathbf{L}^e$ ) and plastic ( $\tilde{\mathbf{L}}^p$ ) components

$$\mathbf{L} = \mathbf{L}^e + \tilde{\mathbf{L}}^p, \quad (10)$$

$$\mathbf{L}^e = \dot{\mathbf{F}}^e (\mathbf{F}^e)^{-1}, \quad (11)$$

$$\tilde{\mathbf{L}}^p = \mathbf{F}^e \mathbf{L}^p (\mathbf{F}^e)^{-1} = \mathbf{F}^e \dot{\mathbf{F}}^p (\mathbf{F}^p)^{-1} (\mathbf{F}^e)^{-1}, \quad (12)$$

where  $\tilde{\mathbf{L}}^p$  is the plastic velocity gradient expressed in the loaded configuration and  $\mathbf{L}^p$  is the plastic velocity gradient expressed in the reference configuration. The plastic velocity gradient in the loaded configuration can be taken as the sum of the rate of stretching and the rate of spin

$$\tilde{\mathbf{L}}^p = \tilde{\mathbf{D}}^p + \tilde{\mathbf{W}}^p, \quad (13)$$

where  $\tilde{\mathbf{D}}^p$  (symmetric tensor) is the rate of plastic stretching and  $\tilde{\mathbf{W}}^p$  is the rate of plastic spin. Without loss of generality, we choose  $\tilde{\mathbf{W}}^p = 0$ . The plastic deformation gradient is then updated by

$$\dot{\mathbf{F}}^p = \mathbf{L}^p \mathbf{F}^p = (\mathbf{F}^e)^{-1} \tilde{\mathbf{D}}^p \mathbf{F}, \quad (14)$$

where  $\tilde{\mathbf{D}}^p$  must be constitutively prescribed.

## 2. Constitutive

The material stress state is related to the elastic deformation by the constitutive law for a linear elastic spring

$$\mathbf{T} = \frac{1}{J} \mathcal{L}^e [\ln \mathbf{V}^e], \quad (15)$$

where  $J = \det \mathbf{F}$  is the volume change,  $\mathcal{L}^e$  is the fourth-order modulus tensor, and  $\ln \mathbf{V}^e$  is the Hencky strain. It is assumed that the material is initially isotropic and can therefore be defined by any two elastic constants. Here, we use the shear modulus  $\mu$  and the bulk modulus  $\kappa$

$$\mathcal{L}^e = 2\mu \mathcal{I} + \left( \kappa - \frac{2}{3}\mu \right) \mathbf{I} \otimes \mathbf{I}, \quad (16)$$

where  $\mathcal{I}$  and  $\mathbf{I}$  are the fourth-order and second-order identity tensors, respectively.

The plastic stretching tensor in the loaded configuration is prescribed as the product of the scalar rate of plastic deformation and a direction tensor

$$\tilde{\mathbf{D}}^p = \dot{\gamma}^p \mathbf{N}^p, \quad (17)$$

where  $\dot{\gamma}^p$  is the scalar rate of plastic strain, and the direction  $\mathbf{N}^p$  is taken to be coaxial with the deviatoric portion of the stress ( $\mathbf{T}' = \mathbf{T} - \frac{1}{3} \text{tr} \mathbf{T}$ )

$$\mathbf{N}^p = \frac{\mathbf{T}'}{|\mathbf{T}'|}. \quad (18)$$

The scalar rate of plastic deformation is constitutively prescribed to follow a rate dependent process driven by the shear stress

$$\dot{\gamma}^p = \dot{\gamma}^o \exp \left[ \frac{-\Delta G}{k_b \theta} \right] \sinh \left[ \frac{\tau_{eff} \Omega}{2k_b \theta} \right]^{\frac{1}{m}}, \quad (19)$$

where  $\tau_{eff}$  is the effective shear stress driving plastic deformation,  $\dot{\gamma}^o$  is a pre-exponential factor proportional to the attempt frequency,  $\Delta G$  is the shear yield activation energy,  $\Omega$  is the plasticity activation volume, and  $m$  is the strain rate sensitivity parameter.  $\tau_{eff}$  is itself a function of several internal variables

$$\tau_{eff} = \tau - s_a - s_b - \beta \bar{p}, \quad (20)$$

where  $\tau = \sqrt{\frac{1}{2} \mathbf{T}' \mathbf{T}'}$  is the scalar equivalent shear stress,  $s_a$  captures the material history effect reflected in the yield peak,  $s_b$  captures isotropic hardening associated with polymer chain alignment,  $\beta$  is the pressure sensitivity coefficient, and  $\bar{p} = -\text{tr} \mathbf{T} / 3$  is the hydrostatic pressure. The rate and history dependent yield peak evolution is governed by following equations:

$$\dot{s}_a = h_a (s_a^* - s_a) \dot{\gamma}^p, \quad (21)$$

$$s_a^* = c_a (\phi^* - \phi), \quad (22)$$

$$\dot{\phi} = h_\phi (\phi^* - \phi) \dot{\gamma}^p, \quad (23)$$

$$\phi^* = z \left( \frac{\dot{\gamma}^p}{\dot{\gamma}_{ref}^p} \right)^r, \quad (24)$$

where  $s_a^*$  is the current target value for  $s_a$ ,  $h_a$  controls the rate of approach of  $s_a$  to its target value,  $\phi$  is a state variable related to molecular mobility,  $\phi^*$  is the rate dependent target value for  $\phi$ ,  $c_a$  scales the yield peak relative to the molecular mobility disequilibrium,  $h_\phi$  controls the rate of approach of  $\phi$  to its target value,  $z$  and  $r$  set the rate dependent value of  $\phi^*$ , and  $\dot{\gamma}_{ref}$  is an arbitrarily chosen reference shear rate. The isotropic strain hardening portion of the response is given by

$$s_b = c_b (\lambda_{ch} - 1), \quad (25)$$

where  $c_b$  is the isotropic hardening slope and  $\lambda_{ch} = \left[ \frac{\text{tr}(\mathbf{F}\mathbf{F}^T)}{3} \right]^{\frac{1}{2}}$  is a scalar description of the material deformation.

The material parameters used to fit the mechanical model to the experimental data are listed in Table I.

## B. Activation model

The activation model relies foremost on the mechanical response as described in Sec. III A. First, a constraint is imposed on the macroscale activation based on the internal state variables of the mechanical model. Activation is only permissible if there is sufficient molecular mobility

TABLE I. Material parameters for continuum mechanical model. # indicates parameter taken directly from Srivistava *et al.* (2009).

Model component	Material parameter	Value
Elastic	$\kappa$	$2.2 \times 10^9$ Pa
	$\mu$	$7.4 \times 10^8$ Pa
Rate dependent yield	$\dot{\gamma}^o$	$6 \times 10^8$ s <sup>-1</sup>
	$\Delta G^\#$	$1.3 \times 10^{-19}$ J
	$\Omega$	0.49 nm <sup>3</sup>
	$m^\#$	0.22
	$\beta^\#$	0.2
Pressure dependent yield		
Distributed yield	$c_a$	$4 \times 10^7$ Pa
	$h_a$	45
	$h_\phi$	60
	$z$	1.0
	$r$	0.3
	$\dot{\gamma}_{ref}$	0.01 s <sup>-1</sup>
Isotropic hardening	$c_b$	$4.5 \times 10^7$ Pa

$$\frac{\phi}{\phi^*} > 0.99, \quad (26)$$

where  $\phi$  and  $\phi^*$  are the internal state variables used in the mechanical plasticity model. Equation (26) is a direct expression of the constraint that the rigid matrix imposes on the mechanophore kinetics as calculated in vacuum with the FMPES-MEP. Second, the continuum mechanical model provides the stress that will drive activation on the local scale.

Local force is assumed to be a function of the magnitude of the continuum shear stress

$$\bar{f} = \hat{g}[\tau], \quad (27)$$

where  $\bar{f}$  is the mean force driving activation and  $\hat{g}$  is a function of  $\tau$ , the effective shear stress calculated from the mechanical continuum model. The effective shear stress is used (rather than the total stress magnitude) in analogy to polymer plasticity modeling with the intent that this model hold for all modes of loading.

Local force is translated into an activation response using transition state theory with parameters calculated from the *ab initio* minimum energy pathway. When force is spatially and temporally uniform, the force driving activation is simply  $f = \bar{f}$ . This force is inserted directly into Eq. (4) through Eq. (7). We expect that there are spatial and temporal force fluctuations not reflected in macroscopic stress measurements. Computationally, this fluctuation is captured as a continually present distribution in force. We assume a normal distribution characterized by the mean force and a standard deviation held at a constant ratio to that force. The normal distribution is discretized into 9 weighted effective force values. This fluctuation is assumed to be temporal with all the effective forces acting to drive the response of a single population within each element. The effective forces and corresponding weights for the discretization are listed in Table II, where  $\Delta f^i$  is a force fluctuation,  $\sigma$  is the standard deviation of the force distribution which will be fit to the experimental data, and  $w^i$  is the weighting factor for each discretized force evaluation.

TABLE II. Discretization of normal distribution of effective forces and corresponding weights.

No.	$\Delta f^i / (\sigma \bar{f})$	$w^i$
1	0	0.3829
2	-0.725	0.1499
3	0.725	0.1499
4	-1.134	0.1359
5	1.134	0.1359
6	-2.184	0.0165
7	2.184	0.0165
8	-2.736	0.0062
9	2.736	0.0062

## IV. RESULTS AND DISCUSSION

### A. *Ab initio* molecular dynamics (FMPES-MEP)

Minimum energy path calculations on the force modified potential energy surface were performed on the SP mechanophore at constant forces of 0 and 0.5 nN (Cremar, 2012). The potential energy surface in these calculations is obtained using density functional theory (Hohenberg and Kohn, 1964) with the B3LYP functional (Becke, 1988) and the 6-31 G basis set (Becke, 1993). The 0 and 0.5 nN force range is small enough that linear interpolation of the SP-MC energy barrier is a good approximation, but large enough to span most of the forces that are experienced by the mechanophores in the simulation. The activation energies and attempt frequencies associated with each of the two pathways (Figure 1) for the forward and reverse reactions are presented in Table III. The SP to MC energy barriers decrease significantly with applied force, whereas the MC to SP energy barriers increase significantly with applied force. The shift in energy barriers results in an increasing percentage of mechanophores in the MC state with increasing force as expected. There is a noticeable change in attempt frequency with increasing force for both of the forward and reverse transformations. Given the weak dependence of rate constants on attempt frequency, these changes in attempt frequency have only a minor effect on either the kinetics or equilibrium state of the mechanophore.

The significance of the *ab initio* FMPES-MEP results for the reaction kinetics is most readily understood in terms of the SP to MC reaction when a constant mean force is

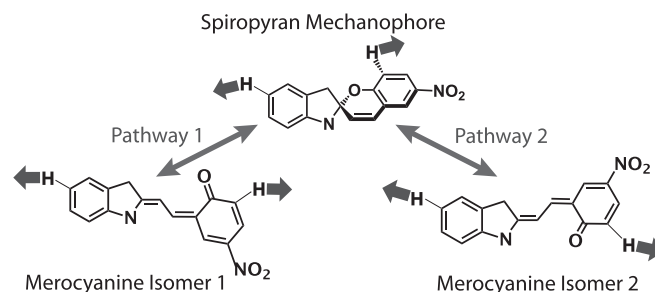


FIG. 1. Two separate reaction pathways exist for activation: spiropyran to merocyanine isomer 1 and spiropyran to merocyanine isomer 2. The pathways have similar but distinct force dependent energy barriers for both the forward and reverse reactions. Both end products fluoresce.

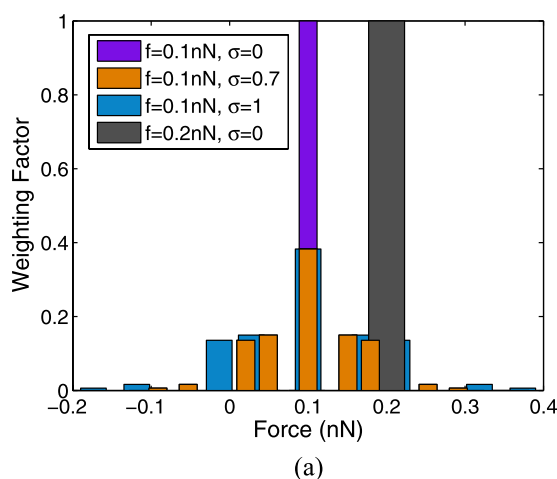
TABLE III. Results from *ab initio* FMPES-MEP simulations of the reversible conversion of SP to MC under constant force.

Force (nN)	$Q_f^\ddagger/Q_f$	$\Delta G_f$ (Jmol <sup>-1</sup> )	$Q_r^\ddagger/Q_r$	$\Delta G_r$ (Jmol <sup>-1</sup> )	Pathway
0	8.59	$1.19 \times 10^5$	0.839	$9.79 \times 10^4$	1
0	9.68	$1.18 \times 10^5$	1.23	$1.04 \times 10^5$	2
0.5	0.798	$5.81 \times 10^4$	0.158	$1.43 \times 10^5$	1
0.5	6.51	$5.96 \times 10^4$	1.63	$1.53 \times 10^5$	2

applied directly across the mechanophore. The activation that occurs over time in response to a constant mean force of 0.1 nN is shown in Figure 2(b). When there is no distribution of force about the mean value, the activation shows negligible increase over the course of 100 s. When this mean force is doubled, activation occurs significantly faster, reaching a value of 0.2 over the course of 100 s. The SP to MC reaction is sensitive to any spatial or temporal fluctuations in the force. Assuming both types of fluctuations are present and of comparable magnitude, temporal fluctuations will mask spatial fluctuations. Two results are shown for increasing temporal fluctuation about the mean force with the activation increasing significantly with increase in the standard deviation of the fluctuation (discretization of each distribution calculated as in Table II is shown in Figure 2(a)). The distribution greatly accelerates the activation under constant mean force, a standard deviation of 0.07 nN results in activation of 0.18 in 100 s and a standard deviation of 0.1 nN results in nearly full activation within 100 s. The strong dependence of activation on force distribution is a direct result of the linear dependence of the transformation energy barriers on force and the exponential dependence of the forward and reverse rate constants on the transformation energy barriers. Even an infrequent occurrence of high force can result in significant activation.

## B. Classical MD

Molecular dynamics simulations of simple shear loading of PMMA crosslinked by 1.15 mol. % EGDMA produce



realistic stress-strain behavior. Figure 3(a) compares the MD results at strain rates of  $10^9$  s<sup>-1</sup> and  $10^{10}$  s<sup>-1</sup> with experimental data from  $10^{-4}$  s<sup>-1</sup> to  $10^{-2}$  s<sup>-1</sup>. The large rate difference between the experimental and MD results is due to the limitation of times accessible to MD simulations. Nonetheless, the MD simulations exhibit the expected elastic response, large yield peak, post yield strain softening, and eventual strain hardening. Additionally, it captures the expected trends with increasing rate: increase in shear modulus, yield peak stress, yield peak strain, and onset of strain hardening at larger strains. This last trend seems more exaggerated than expected and may reflect a deficiency in the simulation setup either due to the size of the unit cell or the relatively simplistic choice of forcefield.

The relationship between macroscopic stress and local force is the primary result from the MD simulations that is needed for the continuum model. Figure 3(b) shows the force across the central EGDMA carbons for the two simulated rates. For both rates, this force follows the macroscopic stress except for the absence of a yield peak. Interestingly, force on the carbons in the PMMA backbone evolves quite differently with macroscopic deformation. The backbone force continues to increase significantly in the post-yield regime, even as the macroscopic stress softens. This indicates that the mechanophore response should be sensitive to the linking architecture. Given these results, Eq. (27) giving the general function ( $\hat{g}$ ) of local force across the crosslinks as a function of shear stress is specified as a simple proportionality

$$\bar{f} = C\tau, \quad (28)$$

where  $C = 2.5 \times 10^{-18}$  m<sup>2</sup>. This fit is plotted as part of Figure 3(b).

## C. Macroscale

The monotonic shear stress-strain behavior is well fit by the mechanical model described in Sec. III A (Figure 4(a)). Critically, this model captures the rate dependence of the magnitude and shape of the yield peak. The evolution of the

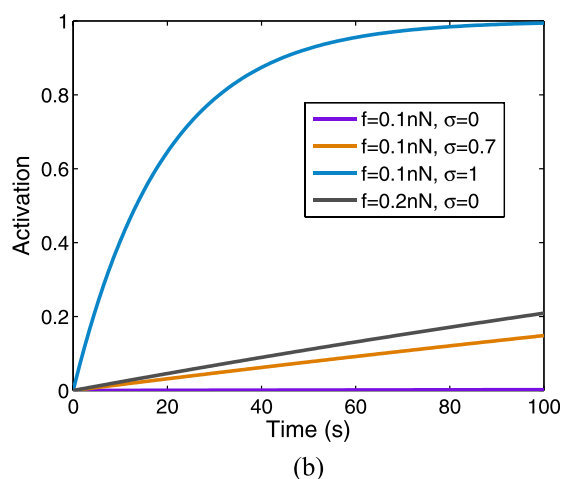


FIG. 2. Kinetics of activation under constant force highlighting the role of force distributed about a mean (a) force distribution (b) activation at constant force resulting from force distribution.  $\sigma$  indicates standard deviation divided by mean force ( $\bar{f}$ ).

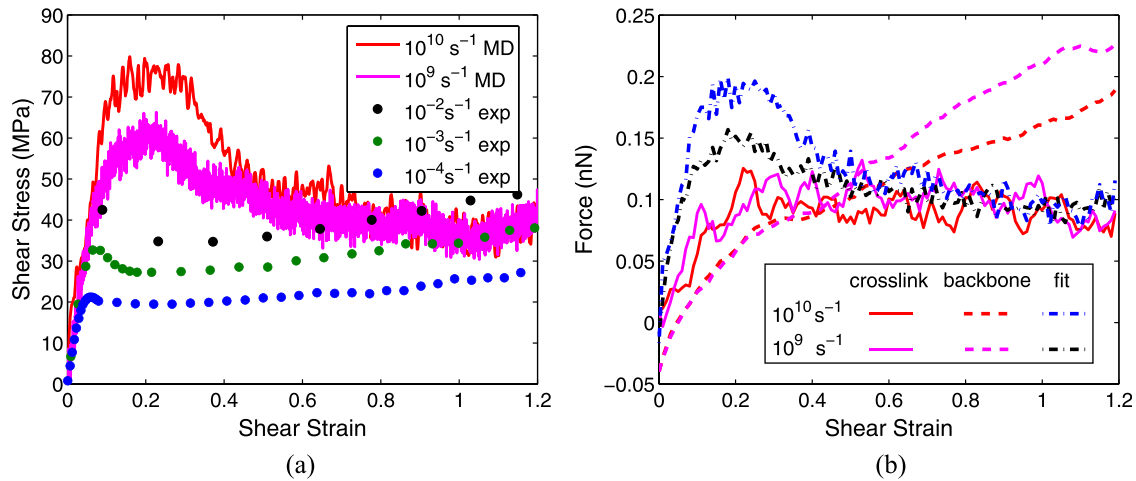


FIG. 3. Response from molecular dynamics simulation of crosslinked PMMA under monotonic simple shear. (a) Shear stress versus shear strain as a function of strain rate with experimental data for reference, (b) Local force versus shear strain for the crosslinks and backbone including result of function used to convert stress to local force.

state variables underlying the post-elastic regime behavior is shown in Figure 4(b). It is readily apparent that  $s_a$  is responsible for the yield peak and that the approach of  $\phi$  to its steady state value defines the end of the yield peak. Recall that the internal state variable  $\phi$  captures the mobility restriction on mechanophore activation such that an effective force is only transmitted to the mechanophore, once it is close to its steady state value.

The activation response to monotonic loading is calculated in conjunction with the mechanical response. Experimentally, activation is independent of strain rate. Activation calculated with no fitting parameters and no force distribution under predicts the experimentally observed behavior and predicts a mild strain rate dependence with the slowest rate having the largest response (Figure 5(a)). Effectively, this set of simulation results indicates that the model parameters underestimate the role of force in accelerating the mechanophore kinetics.

The discrepancies between the model and experiment are addressed by modifying the model to include fluctuations in local force. Glassy polymers exist in a non-equilibrium

state resulting in local force fluctuations whose magnitude has not been well characterized. A standard deviation in the force of 78% of the mean force results in activation that closely matches the experimental data (Figure 5(b)).

Creep loading validates the activation model and further reveals the close tie between activation and plastic deformation. Figure 6 compares the simulation results from the full model to the experimental results at different constant torque values for both strain and activation as functions of time. Four to five experiments are run at each torque value, the samples which exhibit the minimum and maximum creep strain history for each torque are utilized as bounds for the simulation comparison. In each case, the activation response trails the creep strain. The relative slopes of the activation-time response correlate closely with those of the creep strain-time response. The model captures this delayed correlation between the onset of strain softening (accelerating creep) and the onset of activation with the mobility parameter condition (Eq. (26)). There is a slight over prediction of both creep and activation at the lowest torque level, but the model otherwise falls within the experimental bounds, and

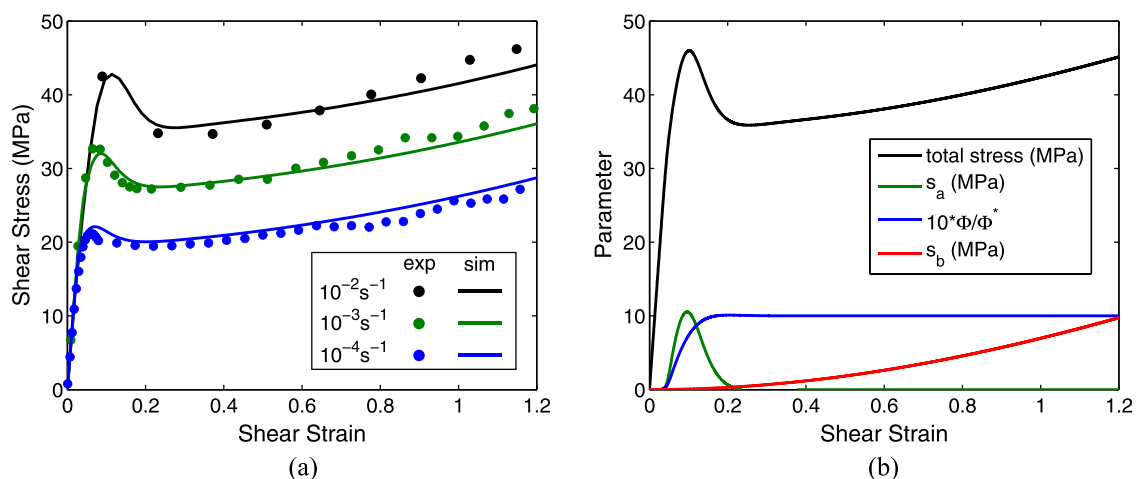


FIG. 4. Experimental and simulated response of SP-linked crosslinked PMMA under monotonic torsional loading. (a) Shear stress vs shear strain at three different strain rates. (b) Representative evolution of state variables related to capturing the yield peak and post yield hardening.

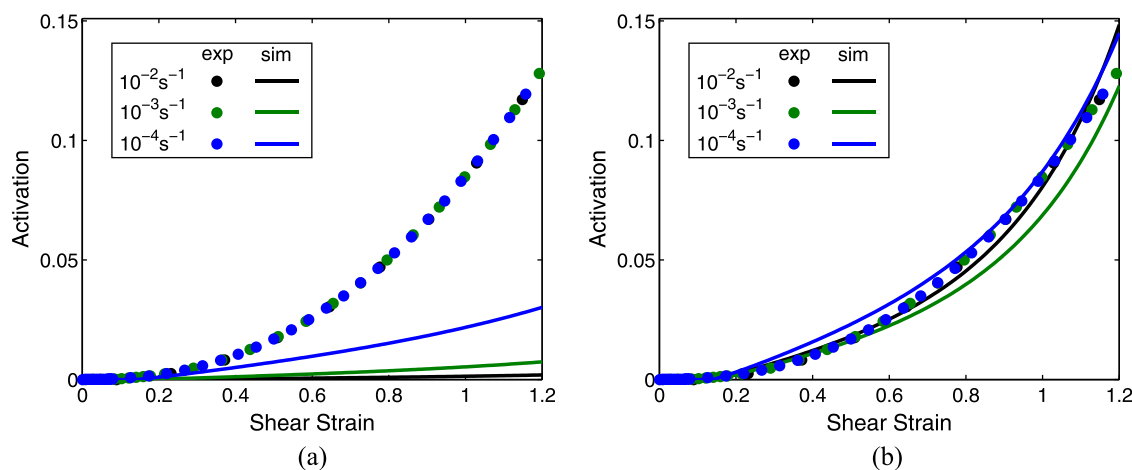


FIG. 5. Experimental and simulated activation response of SP-linked crosslinked PMMA under monotonic torsional loading. (a) Activation vs shear strain for model with no fitting parameters, (b) Activation vs shear strain for model including a force distribution.

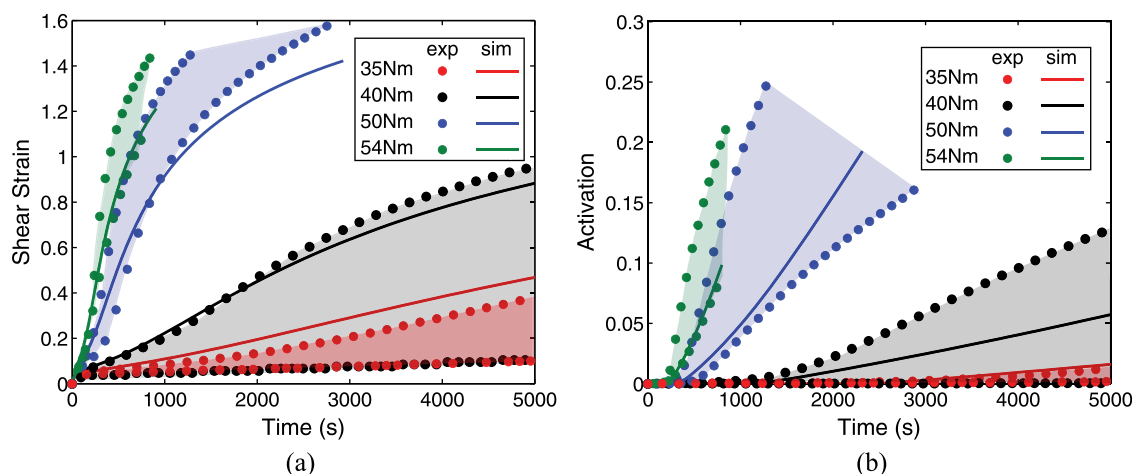


FIG. 6. Experimental and simulated response of SP-linked crosslinked PMMA under constant torque at torque levels below the monotonic yield peak. (a) Shear strain vs time (b) Activation vs time. Experimental data indicate the minimum and maximum of 4–5 experiments conducted at each torque value (35 Nm  $\sim$  20 MPa, 40 Nm  $\sim$  23 MPa, 50 Nm  $\sim$  28 MPa, 54 Nm  $\sim$  31 MPa).

even more critically shows the experimentally determined relationship between the mechanical creep-strain response and the mechanochemical creep-activation response.

## V. CONCLUSIONS

A physics driven continuum model has been developed to describe covalent mechanochemical reactions in glassy polymers. This model quantitatively incorporates *ab initio* FMPES-MEP of local mechanophore kinetics, MD of polymer microscale force transmission, and experimentally observed mechanical behavior. A zero fitting parameter activation model provides a lower bound prediction of the activation with a rate dependence larger than observed experimentally, favoring activation for slower loading. Upon comparison with experimental data, fluctuations in local force are introduced to the model. This modification leads to the model accurately capturing the activation resulting from monotonic loading across three decades of strain rate and from constant torque loading. The success of this model in fitting and predicting a wide range of shear loading histories suggests that the dominant physics is incorporated in the

model. In order to make the model predictive without any reference experimental data, we need to better understand how the effective mean force differs from the stress based mean force.

## ACKNOWLEDGMENTS

This material was based upon work supported in part by the U.S. Army Research Office under Contract/Grant No. W911NF-07-1-0409. M. Silberstein acknowledges the Arnold and Mabel Beckman Foundation postdoctoral fellowship. K. Min acknowledges National Science Foundation Grants 0941497 and 1127480.

- Becke, A. D., "Density-functional exchange energy approximation with correct asymptotic-behavior," *Phys. Rev. A* **38**, 3098–3100 (1988).  
 Becke, A. D., "Density-functional thermochemistry 3. The role of exact exchange," *J. Chem. Phys.* **98**, 5648–5652 (1993).  
 Beiermann, B. A., Davis, D. A., Kramer, S. L. B., May, P. A., Moore, J. S., Sottos, N. R., and White, S. R., "Environmental effects on mechanochemical activation of spiropyran in linear PMMA," *J. Mater. Chem.* **21**, 8443–8447 (2011).

- Bell, G. I., "Models for specific adhesion of cells to cells," *Science* **200**, 618–627 (1978).
- Black, A. L., Lenhardt, J. M., and Craig, S. L., "From molecular mechanochemistry to stress-responsive materials," *J. Mater. Chem.* **21**, 1655–1663 (2011).
- Caruso, M. M., Davis, D. A., Shen, Q., Odom, S. A., Sottos, N. R., White, S. R., and Moore, J. S., "Mechanically induced chemical changes in polymeric materials," *Chem. Rev.* **109**, 5755–5798 (2009).
- Cremer, L. D., "Insights for designing mechanochromic spiropyran from first principles dynamics and minimum energy pathways," Ph.D. dissertation (Stanford University, Palo Alto, CA, 2012).
- Davis, D. A., Hamilton, A., Yang, J., Cramer, L. D., Gough, D. V., Potisek, S. L., Ong, M. T., Braun, P. V., Martinez, T. J., White, S. R., Moore, J. S., and Sottos, N. S., "Force-induced activation of covalent bonds in mechanoresponsive polymeric materials," *Nat. Lett.* **459**, 68–72 (2009).
- Fan, C. F., Cagin, T., Chen, Z. M., and Smith, K. A., "Molecular modeling of polycarbonate. I. Force field, static structure, and mechanical properties," *Macromolecules* **27**, 2383–2391 (1994).
- Hickenboth, C. R., Moore, J. S., White, S. R., Sottos, N. R., Baudry, J., and Wilson, S. R., "Biasing reaction pathways with mechanical force," *Nature* **446**, 423–427 (2007).
- Hohenberg, P. and Kohn, W., "Inhomogeneous electron gas," *Phys. Rev.* **136**, B864–B871 (1964).
- Jaramillo, E., Wilson, N., Christensen, S., Gosse, J., and Strachan, A., "Energy-based yield criterion for PMMA for large-scale molecular dynamics simulations," *Phys. Rev. B* **85**, 024114-1-7 (2012).
- Kauzmann, W. J. and Eyring, H., "The viscous flow of large molecules," *J. Am. Chem. Soc.* **62**, 3113–3125 (1940).
- Kingsbury, C. M., "Multiscale characterization of mechanochemical reactions in mechanophore-crosslinked polymers under shear loading," Ph.D. thesis (The University of Illinois at Urbana-Champaign, Urbana, IL, 2012).
- Kingsbury, C. M., May, P. A., Davis, D. A., White, S. R., Moore, J. S., and Sottos, N. R., "Time-dependent mechanochemical response of SP-crosslinked PMMA" (to be published).
- Lee, C. K., Davis, D. A., White, S. R., Moore, J. S., Sottos, N. R., and Braun, P. V., "Force-induced redistribution of chemical equilibrium," *J. Am. Chem. Soc.* **132**, 16107–16111 (2010).
- Mark, J. E., *Physical Properties of Polymers Handbook* (American Institute of Physics, New York, 1996).
- Mayo, S. L., Olafson, B. D., and Goddard, W. A., "DREIDING: A generic force field for molecular simulations," *J. Phys. Chem.* **94**, 8897–8909 (1990).
- Mulliken, A. D. and Boyce, M. C., "Mechanics of the rate-dependent elastic-plastic deformation of glassy polymers from low to high strain rates," *Int. J. Solids Struct.* **43**, 1331–1356 (2006).
- Nadai, A., *Theory of Flow and Fracture of Solids* (McGraw-Hill, New York, 1950).
- Ong, M. T., Leiding, J., Hongli, T., Virshup, A. M., and Martinez, T. J., "First principles dynamics and minimum energy pathways for mechanochemical ring opening of cyclobutene," *J. Am. Chem. Soc. Commun.* **131**, 6377–6379 (2009).
- Plimpton, S. J., "Fast parallel algorithms for short-range molecular dynamics," *J. Comput. Phys.* **117**, 1–19 (1995).
- Sane, S. B., Cagin, T., Knauss, W. G., and Goddard III, W. A., "Molecular dynamics simulations to compute the bulk response of amorphous PMMA," *J. Comput. Aided Mater. Des.* **8**, 87–106 (2001).
- Silberstein, M. N., Cremer, L. D., Beiermann, B. A., Kramer, S. B., White, S. R., Martinez, T. J., and Sottos, N. R., "Modeling mechanophore activation within a viscous rubbery network" (personal communication).
- Srivastava, V., Chester, S. A., Ames, N. M., and Anand, L., "A thermo-mechanically coupled large-deformation theory for amorphous polymers in a temperature range which spans their glass transition," *Int. J. Plast.* **26**, 1138–1182 (2010).
- Wu, H. C., Xu, Z., and Wang, P. T., "The shear stress-strain curve determination from torsion test in the large strain regime," *J. Test. Eval.* **20**, 396–402 (1992).